Recent interannual upper ocean variability in the deep southeast Bering Sea

by Amy E. Wirts[1,2] and Gregory C. Johnson[3]

Submitted to the Journal of Marine Research

10 AUGUSt 2004

Revised for the Journal of Marine Research

28 OCTOBER 2004

[1] School of Oceanography, University of Washington, Seattle Washington 98105, U.S.A.

[2] Present affiliation: US Coast Guard Academy, New London Connecticut 06320, U.S.A., e-mail:awirts@cga.uscg.mil

[3] Corresponding author: NOAA/Pacific Marine Environmental Laboratory, 7600 Sand Point Way Bldg. 3, Seattle Washington 98115, U.S.A, e-mail: gregory.c.johnson@noaa.gov

ABSTRACT

Recent seasonal and interannual variability of the upper ocean in the southeast Aleutian Basin of the Bering Sea is related to air sea fluxes, ocean advection, and mixing. Between the winter of 2001/2002 and that of 2002/2003 a warming and freshening of the upper ocean was observed in data from a regional array of profiling Conductivity-Temperature-Depth (CTD) floats. The mild winter of 2002/2003 resulted in an unusually warm, fresh, light, and shallow winter mixed layer and a weakly ventilated temperature minimum layer. These unusual winter conditions contributed to a substantial reduction in the subsurface temperature inversion characteristic of the southeast Aleutian Basin. Heat budget analysis, one dimensional upper ocean model runs, and altimeter sea-surface height anomalies suggest that a combination of atypical ocean advection and anomalous atmospheric forcing contributed to the unusual upper ocean conditions in 2002/2003. The observed warming and disappearance of the temperature minimum in 2002/2003 appears to have preconditioned the water column towards a similar structure in 2003/2004, despite a return to more normal atmospheric forcing.

1. Introduction

The Bering Sea is a semi-enclosed sub-Arctic marginal sea with communication to the North Pacific through passes and straits in the Aleutian Island Arc and with the Arctic through the Bering Strait (Figure 1). Circulation in the deep basin is cyclonic (Stabeno et al., 1999) with warm, salty, nutrient-rich water entering from the south through several passes, and, after significant air-sea exchange within the basin (Miura et al., 2002; 2003), exiting as colder, fresher water in a western boundary current (Stabeno and Reed, 1994). This inflow also fuels productivity in the Aleutian Islands, the eastern shelf of the Bering Sea, and northward into the Chukchi Sea (Stabeno et al., in press). Three major interconnected current systems form the cyclonic gyre in the basin. Relatively warm, salty, and nutrient-rich Alaskan Stream water enters from the North Pacific into the Bering Sea primarily through Near Strait, Amchitka Pass, and Amukta Pass. Most of this water feeds the narrow, eastward flowing Aleutian North Slope Current (ANSC) observed along the north slope of the Aleutian Islands (Reed, 1990; Reed and Stabeno 1994; 1999). The broad, eddy-rich, northwestward flowing Bering Slope Current (BSC; Kinder et al., 1975; Johnson et al., 2004) flows from the southeast corner towards the northern apex of the deep Bering Sea. Finally, the southward flowing Kamchatka Current, the western boundary current, returns relatively cold and fresh water from the Bering Sea to the North Pacific through Kamchatka Strait (Stabeno and Reed, 1994).

Observations historically reveal a seasonal subsurface temperature minimum (T-min) overlaying a deeper temperature maximum (T-max) in the southeast Aleutian Basin (Sayles et al., 1980; Reed, 1995; Roden, 1995; Cokelet and Stabeno, 1997). This temperature inversion is sometimes called the mesothermal structure, with the T-min referred to as dichothermal water and the T-max as mesothermal water (Takenouti and Ohtani, 1974; Endoh et al., 2004). The

deep subsurface T-max in the Aleutian Basin is maintained by lateral inflow of warm Alaskan Stream water through the passes (Cokelet and Stabeno, 1997). Variability in the properties of the layer is thought to result mainly from variations in the strength of inflow through Amukta Pass (Reed, 1995). Historical temperature, depth, and density ranges of the T-max in the southeast Aleutian Basin as determined from 23 years of hydrographic surveys are 3.5 ^{o}C to 4.6 ^{o}C, 150 m to 400 m, and 26.7 kg m^{-3} to 26.9 kg m^{-3} (Reed, 1995).

The properties of the T-min layer reflect the regional late winter mixed-layer properties in the southeast Aleutian Basin (Cokelet and Stabeno, 1997). By late winter, a deep, cold, relatively salty and dense winter mixed layer has formed. In spring, increased insolation and decreased wind stress form a shallow seasonal thermocline over the winter mixed layer, leaving the T-min layer below. Observational evidence of this process is found in mooring data showing a strong cooling episode in February 1994 followed by the appearance of a prominent T-min layer which persisted from April through August at depth ranging between approximately 75 m and 225 m and average density of 26.6 kg m^{-3} (Cokelet and Stabeno, 1997).

2. Data Collection and Methods

Oceanographic data are collected from an array of 14 Webb Research corporation APEX-260 profiling floats equipped with Seabird Electronics Incorporated SBE-41 CTDs. The floats were deployed in the Aleutian Basin between May 2001 and August 2002. The instruments are programmed to drift at pressure of 1000 dbar for 10 days, rise to the surface collecting temperature and salinity data at 60 predetermined pressures over the course of approximately 3.5 hours, and remain at the surface for approximately 11 hours. While on the surface the floats transmit temperature, salinity and pressure data via satellite and several fixes of float positions

are determined by satellite positioning. Every fourth cycle, the floats descend from their park pressure of 1000 dbar to a maximum pressure of 2000 dbar 6 hours prior to rising to the surface. During the extended ascents, data are collected at 70 predetermined pressures. The floats remain at the ocean surface for approximately 7 hours for data transmission and position fixes before descending again to the park pressure. The float data have increasingly high vertical resolution with decreasing pressure. The floats shallowest measurement are programmed to be taken at 5 dbar, with 4-dbar resolution to 55 dbar, then 5-dbar resolution to 150 dbar, 10-dbar resolution to 300-dbar, 20-dbar resolution to 400-dbar, 50-dbar resolution to 600-dbar, and 100-dbar resolution at pressures greater than 600 dbar. Small adjustments are made to float-measured salinities following procedures similar to, but slightly simpler than, those of Wong et al. (2003).

The floats collected 1143 profiles between 29 May 2001 and 24 October 2004 in the Bering Sea (Figure 1). The analysis here focuses on the southeast Aleutian Basin, where there are between 12 and 32 profiles per month between June 2001 and September 2004. Data are presented both as raw values south and east of the thick line in Figure 1 and also as maps of the data at 55^{o}N, 174^{o}W (Figure 1, pentagram). This location is in a relatively data-rich area in the basin interior, away from boundary currents (Johnson et al., 2004).

The maps are made using a 3-dimensional locally weighted quadratic regression, known as a loess filter (Cleveland and Devlin, 1988). The spatial and temporal half-power points of the filter are 10^{o} latitude, 20^{o} longitude, and 60 days. Maps are shown from the start of August 2001 through the middle of August 2004. These dates are far enough from the temporal edges of the data set to avoid end effects. The loess-filtered values will be referred to as mapped data, or simply as the map. The map sometimes masks important short-term variability, so both the map and raw data values are presented when necessary. For example, the map smoothes the rapid

spring transition between the deep, cold winter mixed layer and the much shallower warm summer mixed layer, making it appear to be much more gradual than it actually is. In addition, the mapped winter mixed-layer depth is really the average of deep mixing values driven by wind-mixing and heat loss, and intermittent shallow values associated with surface freshening, likely from precipitation.

The focus of this study is on water column stability and structure, T-min and T-max formation and maintenance, and upper ocean dynamics. For these purposes, data analyses are primarily performed on isopycnals in order to eliminate the effects of isopycnal heaving that can smear water property signatures in isobaric data processing (Lozier et al., 1995), and to allow for observation of the interactions among density layers. For most graphics the isopycnal analyses are remapped onto isobars and plotted vs. pressure. Potential density anomaly referenced to the ocean surface, σ_θ, in kg m^{-3} is used here as the density coordinate. Mixed-layer pressure is defined as the pressure at which σ_θ exceeds the near-surface (5-dbar) value by 0.02 kg m^{-3}. Since this density increase is roughly equivalent to a salinity increase of only 0.025 or a temperature increase of only 0.16°C, the 5-dbar values of temperature and salinity are used to characterize the mixed-layer properties.

The atmospheric forcing parameters used in this study are the National Center for Environmental Prediction / National Center for Atmospheric Research (NCEP/NCAR) reanalysis surface flux products (Kalnay et al., 1996; Kistler et al., 2001; http://www.cdc.noaa.gov/). The website provides both daily and 6-hourly averaged data fields on a 2.5 latitude by 2.5 longitude grid. Daily average values for surface fluxes of shortwave and longwave radiation, sensible heat, latent heat, zonal momentum, meridional momentum, and precipitation are used in section 5 for a climatological analysis of seasonal means, mostly interpolated to 55°N, 174°W (the map

location in the interior of the southeast Aleutian Basin). Evaporation rate is inferred from the latent heat flux values. These fields are also used to force a one-dimensional mixed-layer model in Section 6, except that 6-hourly momentum flux averages are used to force the model, to better account for the influences of fast-moving storms in the region.

Gridded multi-mission sea-surface height anomaly (hereafter SSHA) maps (Ducet et al., 2000) are used to detect circulation anomalies in the region. The monthly averaged Delayed-Time Maps of Sea Level Anomaly (DT-MSLA) maps from CLS Space Oceanography Division (http://www.aviso.oceanobs.com) are used here. These anomalies are estimated relative to a 7-year (1993-1999) mean SSH, and the maps are objectively interpolated from Topex/Poseidon Jason-1, Geosat -Follow-On, and Envisat (or ERS-1, 2 depending on the date) altimeter data. While the standard corrections, including tide removal, are applied to the data, near-coastal data should be viewed with caution.

3. The Upper Ocean Structure

The southeast Aleutian Basin mixed-layer properties (Figure 2) are set by the seasonal cycle of atmospheric forcing as well as lateral advection and mixing. Float data suggest mixed-layer temperatures vary seasonally from approximately 2^{o}C to 5^{o}C in winter and 7^{o}C to 11^{o}C in summer dependent on year and float location. Float mixed-layer salinity values range from 32.1 to 33.4 depending on season and location. The mixed-layer salinity distribution is definitely skew, with a few very fresh values contrasting with a greater number of saltier ones. The fresh values are especially prominent in summer, likely owing to precipitation events under condition with little vertical mixing (little ocean heat loss and wind stress). The fresh values are well correlated with shallow mixed-layer depths, supporting this argument. Similarly, clusters of

salty mixed-layer values, associated with larger mixed-layers depths, are most obvious in winter, likely owing to entrainment of more uniform and saltier halocline waters from below by deep mixing.

The generally weak contribution of temperature to density at the range of temperatures in the Aleutian Basin allows variations in salinity to dominate the upper ocean density structure throughout most of the year. The exception is in the seasonal thermocline where significant summer surface warming dominates the stratification.

Mixed-layer water in the Aleutian Basin is warmest and freshest in the summer months when insolation thermally stratifies the upper water column, creating a shallow seasonal thermocline and a shallow mixed layer (Figure 2). A long-term seasonal analysis of the NCEP/NCAR reanalysis product interpolated to 55^{o}N, 174^{o}W (not shown) suggests a summer maximum in the net surface flux of freshwater into the ocean. This apparent seasonal maximum, coupled with the lack of vertical mixing in the summer, creates a fresh lens at the surface, which reinforces the preexisting temperature stratification by decreasing mixed-layer density. The mixed layer is coldest and saltiest in the winter months when strong storms cool the surface, impart momentum to the upper ocean, and generate high levels of evaporation. The result of surface cooling and mixing is the formation of a cold, dense, and deep winter mixed layer. Mixed-layer density is further increased by the vertical entrainment of relatively salty water from the permanent halocline.

The persistent deep T-max (historically from 3.5 to 4.6 ^{o}C and between 150 and 400m; Reed, 1995) is obvious year round in the map (Figure 3) through most of the time period. Above the T-max, the seasonal T-min (2.5 to 3.5 ^{o}C) is usually evident at 150 to 200 dbar. The strong permanent halocline and corresponding pycnocline begin beneath either the winter mixed layer

or the T-min (150-200 dbar) and rapidly weaken with increasing pressure. The permanent thermocline begins significantly deeper, at the base of the T-max.

A region of diffusive instability exists within the temperature inversion between the T-min and T-max in the southeast Aleutian Basin (Figure 3). The strength of this instability can be quantified using the Turner Angle (Ruddick, 1983). Turner Angles between -90^{o} and 90^{o} indicate a statically stable water column. Within the region of static stability, the potential for diffusive instability begins at -45^{o}, with a theoretical threshold for strong diffusive instability at -71.6^{o}. Tendency towards significant diffusive instability between the T-min and T-max reflects a strong temperature inversion (Figure 4). This tendency is strongest near $\sigma_{\theta} = 26.65$ kg m^{-3}.

4. Interannual Variability

Mixed-layer temperature anomalies (Figure 5) in the southeast Aleutian Basin are determined by removing annual and semiannual harmonics fit to the data (see Figure 2). To highlight changes, the result is smoothed with a loess-filter with a half-power point of one year. This analysis suggests a gradual warming of about 1^{o}C between May 2001 and September 2003, and then a slight cooling over the winter of 2003/2004, entirely reversed by warming near the end of the record. The year-to-year increase in mixed-layer temperature appears in both the smoothed and raw data indicating that this regional warming pattern is a robust interannual time-scale phenomenon. Subsurface water property tendencies include an expanding and warming T-max layer, and a shrinking and warming T-min layer (Figure 3).

Mixed-layer salinity anomalies (Figure 5) calculated in the same fashion as those for temperature suggest a freshening over the winter of 2002/2003. These fresh conditions continue through the end of the record. The raw data show a greater spread of salinity values in the latter

part of the time series, with more very fresh values. The mixed-layer freshening may be a response to the decreased depth and density of mixing in the winter of 2002/2003, and lack of cold, salty water entrainment from below. Subsurface, salinity increases during the winter of 2002/2003 on isopycnals between 26.6 and 27.1 kg m^{-3} (Figure 3).

Winter 2001/2002 had the coldest, saltiest, densest, and deepest mixed-layer values in both the raw values and the map (Figures 2, 3). The raw data show a mixed layer as deep as 200 dbar in winter 2001/2002, although the maximum map mixed-layer depth was 170 dbar. Synoptic precipitation events create temporary shallow fresh mixed layers that skew the mapped data to shallower mixed-layer depths, so that the raw data are more indicative of the maximum extent of winter mixing. In winter 2002/2003 mixed-layer temperatures increased, mixed-layer salinities and densities decreased, and mixed-layer depths decreased compared with the winter of 2001/2002. The mixed-layer depth for 2002/2003 falls between 120-150m, with raw data indicating more frequent synoptic freshening events, as represented by individual shallow data points (Figure 2). These changed mixed-layer conditions in winter 2002/2003 only weakly renewed the T-min layer. In winter 2003/2004, the mixed-layer temperatures were in between values for the two preceding winters. Although some raw mixed-layer values are as deep as in 2001/2002, the mapped values are relatively shallow because of frequent shallow fresh winter mixed layers. Similar to 2002/2003, the 2003/20004 winter mixed layer was only associated with a weakly ventilated T-min layer.

The T-min is defined here as the coldest water under which warmer water, the T-max, exists. At least partly because the densest isopycnals ventilated in winter 2002/2003 and 2003/2004 were lighter than those ventilated in winter 2001/2002 and the previous winter, potential temperature at the T-min and T-max increased significantly between 2001 and 2004

(Figures 3 and 6). The increase in temperature in both layers was accompanied by increased salinity at the T-min and decreased salinity at the T-max. The T-max properties in the early float data lie within the previously reported ranges of temperature and depth (Reed, 1995). More recently, some temperatures exceed the previously documented maximum of 4.6°C (Figure 6), and the layer has expanded in the water column, encompassing pressures between 115 dbar and 380 dbar (Figure 3). Consistent with the erosion of the layered vertical structure, there is an increased number of profiles during 2003 where the vertical temperature gradient is monotonic, indicating that there is neither a subsurface T-min nor a subsurface T-max.

Temperature at σ_θ = 26.6 kg m^{-3}, the historical density of the T-min in the southeast Aleutian Basin (Cokelet and Stabeno, 1997), displays evidence of a seasonal cycle in 2001 and 2002 (Figure 7) with the coldest temperatures occurring in the early summer just after the surface stratification caps the cold winter mixed layer. The mean temperature at σ_θ = 26.6 kg m^{-3} was 3.2 °C during 2002. This isopycnal was not locally ventilated in winter 2002/2003 or in winter 2003/2004, resulting in unusually warm temperatures at this density level from 2003 into 2004. The mean temperature on that isopycnal during 2003 was 3.5°C. Raw temperatures in excess of 4.0°C were sampled for most of the time period, with a maximum of 4.7°C. The increasing temperatures on this isopycnal reflect the effective absence of the T-min during most of 2003. In addition to the observed warming, the isopycnal also moved deeper in the water column between the two winters (Figure 7), suggesting a build-up of lighter, warmer waters above. Mean potential temperature at σ_θ = 26.6 kg m^{-3} remains warm into 2004, well above the historical temperature of the T-min.

Changes in the water-mass structure are also evident in the θ-S diagrams for 2002 and 2003 (Figure 6). The 2003 θ-S curve displays a pronounced shift towards warmer, saltier values

around $\sigma_\theta = 26.6$ kg m^{-3}, the historical location of the T-min. It will be argued below that the virtual disappearance of the T-min from one year to the next is reflective of increased inflow of warm, fresh surface water, and warm, salty Alaskan Stream water throughout the upper water column.

A strongly delineated vertical structure of a cold T-min overlying a warm T-max is conducive to strong diffusive instability. In the absence of renewing factors for both layers, the temperature inversion between the two layers will mix away, eventually vanishing. In 2002 the mean Turner Angle at $\sigma_\theta = 26.65$ kgm^{-3} was -53^o with a few individual values lying beyond the threshold for strong diffusive instability at -71.6^o (Figure 4). In comparison, the mean Turner Angle at the same isopycnal in 2003 was -45^o, just at the threshold for weak diffusive instability. Additionally, there were far fewer Turner Angles suggesting strong diffusive instability. In early 2004, mean Turner Angle on this isopycnal was outside the region of diffusive instability, with no values lying beyond the threshold for strong diffusive instability. Changes in the Turner Angle reflect a significant reduction, if not elimination, of the temperature inversion. Diffusive mixing may have played a role in eroding this structure below by enhanced exchange of heat between the T-min and T-max.

5. Atmospheric Processes

The seasonal cycle of atmospheric forcing over the Aleutian Basin has an enormous impact on the upper ocean water properties. Although atmospheric forcing and subsequent vertical processes are not the only mechanisms that influence the structure of the upper ocean, they are very important to formation of the T-min. The NCEP/NCAR gridded reanalysis fields described in section 2 are used to explore variations in air-sea fluxes. These products are

considered most accurate for the period from 1979 to the present, due to the addition of global satellite data to the reanalysis. Time series from winter 1958/1959 through 2003/2004 are displayed for completeness, with means for the entire period, pre-1979, and post-1979 periods.

Net heat flux into the ocean is quantified by the sum of incoming radiation and outgoing heat fluxes, with a positive sign here indicating heat gain by the ocean. Incoming radiation is a purely radiative flux, consisting solely of shortwave radiation. Net outgoing heat flux includes both radiative and non-radiative heat fluxes, and is defined as the sum of outgoing long wave radiation, latent heat flux, and sensible heat flux. This work focuses on the mean cooling season because of the effect of heat loss on the T-min formation. This season is defined to be 21 September – 10 April using zero-crossings of the seasonal cycle resulting from annual and semiannual harmonics fit to the reanalysis net heat fluxes from winter 1958/1959 through winter 2003/2004. Cooling season heat flux does not display a coherent trend over the record (Figure 8). There is no discernible signal with the change in sign of the Pacific Decadal Oscillation (PDO; Mantua et al., 1997) in 1977. However, the 2002/2003 cooling season is one of the weakest in the record, with only three seasons since 1979 having less heat loss: 1978/1979, 1986/1987, and 1995/1996. Close inspection of the individual terms from the reanalysis contributing to the net heat flux (not shown) reveals that the decreased cooling in 2002/2003 was due to a decrease in latent heat flux rather than a change in shortwave radiation, consistent with the weak wind stress for that season (Figure 8). Cooling in 2003/2004 returned to being stronger than the mean, with heat loss from the ocean similar to 2001/2002.

Wind stress variability is another important factor in determining the depth and temperature of the winter mixed layer, and hence contributes to the T-min formation. The latent heat loss related to increased wind stress induces static instability and overturning of the water

column. The wind also imparts momentum to the upper ocean, resulting in mixing which can help to create a deep, cold, and dense winter mixed layer. The magnitude of the surface momentum flux

$$\tau = [(\tau^x)^2 + (\tau^y)^2]^{1/2} \quad (1)$$

is here estimated from the daily average reanalysis zonal and meridional momentum fluxes, τ^x and τ^y, both in N m^{-2}.

Unlike heat fluxes, cooling season wind stresses do appear higher before 1977 than after, consistent with the change in the PDO leading to less stormy conditions after 1977, but this apparent shift is rendered uncertain by the 1979 advent of satellite data assimilation in the reanalysis. At any rate, the wind stresses during the 2002/2003 cooling season are weak compared to the climatological mean values (Figure 8). The 2002/2003 mean wind stress is the lowest in the time series. Since 1979, only the winters of 1982/1983 and 1986/1987, both El Niño years, were comparably calm. Mean wind stress in 2003/2004 displays the first values above the mean since 1998/1999. The stronger winds in 2003/2004 agree with the greater ocean heat loss for that cooling season.

The net freshwater flux through the ocean surface is also important to evolution of upper-ocean water-mass properties, but NCEP/NCAR reanalysis precipitation product is highly uncertain, so long-term variability of cooling season freshwater flux is not discussed here.

Cooling season NCEP/NCAR reanalysis sea-surface temperature (SST) product values (Figure 9) are at least weakly correlated with cooling season heat flux values (Figure 8), as might be anticipated. Warm SSTs (including 2002/2003 values) are usually associated with weak heat fluxes. Notable post-1979 exceptions are 1979/1980, 1983/1984, and 2003/2004, all of which were preceded by a warm winter with weak ocean cooling. It seems likely that the warm SST

values in these following winters are the result of anomalous heat storage from the previous winters that re-emerge during deep winter mixing (Deser et al., 2003).

The cooling season SST for 2003/2004 is one of the two warmest values since 1979. The relatively strong ocean heat loss and strong wind stress in 2003/2004 suggest a greater loss of heat from the water column, and should translate to cooler SSTs; just as the reduced cooling and wind stresses in 2002/2003 translated to warmer SSTs. However, in this case float CTD observations support the argument that this warmth in the face of normal winter heat fluxes may be a result of the absence of the T-min layer from the previous winter, which would normally reemerge to cool the surface.

Although much of the change in the mixed-layer properties and the weak T-min of 2002/2003 can be attributed to anomalous atmospheric conditions, the anomalous forcing may not account for all of the warming observed in the subsurface layers. A heat budget analysis of the upper water column over the full course of the data set (Moisan and Niiler, 1998) quantifies the differences. Heat content, HC, (in J m^{-2}) for the upper water column is defined as

$$\mathrm{HC} = \int_{z'}^{0} \rho \cdot C_p \cdot T \; \partial z \tag{2}$$

where ρ is density (kg m^{-3}), C_p is specific heat capacity (J kg^{-1} $^{o}C^{-1}$), T is temperature (^{o}C), and z' is the maximum depth (m) of atmospheric influence. Air-sea fluxes certainly do not have local influence below σ_θ = 26.7 kg m^{-3}. Upper ocean heat content estimates (Figure 10) were calculated from the surface to this isopycnal in order to capture all atmospherically forced variability in the upper water column. These estimates are normalized to a uniform depth by dividing each by the individual depths of that isopycnal and multiplying by the mean isopycnal depth for all the profiles. This quantity (Figure 10) was mapped to 55^{o}N 174^{o}W using the loess filter with the same space and time half-power points detailed previously.

In the absence of errors, any difference between the local upper ocean heat content and time-integrated atmospheric heat flux (Figure 10) should primarily reflect advection and mixing of heat into the analysis region. The residual over the period of integration is equivalent to a 20 Wm^{-2} surface heat flux between August 2001 and August 2004. Of course this discrepancy between atmospheric input and the upper ocean heat content could simply indicate errors in the NCEP/NCAR reanalysis heat flux product at the map location. However, the increased temperature and vertical extent of the T-max suggest that a circulation anomaly importing warm water into the region likely accompanied the air-sea flux anomalies augmenting the erosion of the T-min in 2002/2003. Variability in the position of the Alaskan Stream with respect to the Aleutian passes and straits is known to influence transport through these gaps and therefore circulation and water properties in the Aleutian Basin (Reed, 1995; Stabeno et. al, 1999), as discussed below.

6. Ocean Circulation Anomalies

Bond and Adams (2002) found that negative (easterly) anomalies in the along-peninsula wind stress value at 53°N 173°W coincide with increased (eastward) transport in the Aleutian North Slope Current. Their proposed mechanism for this circulation anomaly is a shift in the position of the Alaskan Stream due to the along-peninsula wind changes. The along-peninsula wind stress value for the 2002/2003 cooling season (Figure 11) fell considerably from values over previous winters, suggesting that a positive circulation anomaly may have carried warm water into the Southeast Aleutian Basin. Stabeno and Reed (1992) estimated that the migration of the Alaskan Stream away from the Aleutian Chain resulted in nearly zero transport of the warm subsurface waters into the basin between summer 1990 and fall 1991. The claimed effect

of the circulation anomaly was a 0.5°C cooling of the subsurface layers. It seems plausible that the subsurface increase in heat content observed in the southeast Aleutian Basin could be largely accounted for in the expansion of the deep T-max due to anomalously strong transports from the Alaskan Stream into the basin.

Monthly SSHA maps from October 2002 through January 2003 (Figure 12) provide further evidence for a basin-wide circulation anomaly that coincides with the strengthening of the temperature maximum. The use of data from four altimeters and the monthly averaging may partly ameliorate the problem of tidal and other noise, but signals near the coast described below should still be viewed with caution. In October 2002, SSHA values are near normal inshore of the 1000-m isobath north of Vancouver Island, in the Gulf of Alaska, and on the eastern shelf of the Bering Sea. In November, near-shore SSHA values are elevated in the Gulf, but not on the Bering Shelf. In December, elevated values build inshore of the shelf break throughout the Gulf and on the Bering Shelf. This pattern continues in January 2003, but collapses in February 2003 (not shown). Examination of monthly maps from 1993 through 2003 (not shown) reveals a similar pattern in a few other winters, but not since the winter of 1997/1998. That winter is the only other one with as strong a SSHA pattern, another El Niño year, and one with strong easterly along-peninsula wind stresses (Figure 11).

The strong gradient in SSHA perpendicular to the shelf break during these months suggests stronger geostrophic currents northward from the Gulf into the Bering Sea. This change could be the result of a locally or remotely driven coastally trapped wave or, alternately, anomalous heating over, freshening on, or mass flux onto the entire shelf in the sub polar North Pacific. The elevated SSHA onshore and depressed values offshore causing this gradient were found at the time of the apparent influx of warm water into the basin (the T-max strengthening

and expansion; Figure 3). The strengthening of the Alaskan Stream and cyclonic circulation in the deep Bering Sea implied by the SSHA in winter 2002/2003 could supply warm water into the southeast Aleutian Basin to serve as the mechanism for the expansion of the T-max layer.

7. Modeling

A one dimensional upper ocean model (Price et al., 1986, hereafter PWP) is used to explore further the impact of atmospheric variability on the upper ocean water properties observed by the floats. Because only vertical processes are modeled by PWP, it should allow study of the influence of local air-sea fluxes alone on the ocean structure. The model is forced with NCEP/NCAR reanalysis surface flux product interpolated to 55^{o}N 174^{o}W and the model time-step. Daily means of the products are used with the exception of wind stress. The six-hourly mean wind stress product is used to account for synoptic storm variability that might be reduced in the daily mean value. Three model runs are initialized with temperature and salinity profiles mapped to 55^{o}N 174^{o}W on 01 September 2001, 2002, and 2003, respectively, with the loess filter. Each is integrated for a year. Upwelling velocities from the curl of the 2.5^{o} by 2.5^{o} wind stress product were added to the model. To model the Ekman suction simply in the one-dimensional slab model, upwelling is set to zero at the surface and increases linearly to a maximum at the mixed-layer depth, then decreases linearly to zero velocity at 1000 dbar, the bottom of the model domain (Schudlich and Price, 1992). The vertical mixing coefficient (K_z) is set at $5x10^{-5}$ for all model runs. A series of four-month model runs (not shown) were used for tuning K_z so the model best reproduced observations.

The NCEP/NCAR reanalysis product seems adequate for broad scale analysis of anomalies in seasonal and interannual variability. However, comparison of model results (Figure

13) to observations (Figure 3) suggests that the magnitude of the reanalysis heat flux product cycle in the southeast Aleutian Basin may be too large with respect to the upper ocean data. The model creates a winter mixed layer (Figure 13) noticeably colder than the observations (Figure 3), and a summer mixed layer that is warmer than observed. Reanalysis heat flux errors have previously been found in the region by comparison with in situ observations (Ladd and Bond, 2002). In addition, the reanalysis seasonal air-sea freshwater flux product variability is about half the magnitude needed to adequately reproduce the observed upper ocean cycle. However, lateral advection could account for at least some of these discrepancies.

Comparison of model results to observations also suggests the reanalysis wind stress product values may be too weak in winter. The winter model mixed-layer temperatures, colder than observations, may be partly a result of too-weak vertical mixing in the model from under-estimated reanalysis wind stress products which result in a model mixed layer that is shallower than observed and fails to distribute the heat loss deeply enough in the water column. Modeled vertical mixing in winter 2001/2002 extends to only approximately 125 dbar, compared with the observed mixed-layer depth of 175-200 dbar. The mixed-layer depth in winter 2002/2003 extends to approximately 125 dbar again, closer to the observed mixed-layer depth for that winter. However, the mixed layer is still much colder and denser than observed. In winter 2003/2004 the model creates a mixed layer which extends to 100 dbar, close to the map value of mixed-layer depth, but again, much shallower than the observed raw values of 175-200 dbar.

The lack of lateral processes (advection and mixing) in the model allows vertical structures present in the initial model profile to persist much longer than they actually endure in the ocean observations. The model also does not take into account any increases in vertical mixing owing to diffusive instability within temperature inversions. In 2002/2003 the 3^{o}C T-min

is sustained in the model (Figure 13) until the onset of winter mixing in January 2003, so that vertical mixing entrains water from below that is colder than observed (Figure 3). The entrainment of the cold subsurface water intensifies the already low mixed-layer temperature. In the ocean, the lateral inflow of warm T-max water normally moderates the coldest T-min temperatures before the maximum winter mixed-layer depth is reached. The absence of this warm inflow in the model, and perhaps the absence of enhanced diffusive instability mixing in the vertical, allows the T-min to persist throughout the full year in multi-year runs (not shown) and build on itself interannually, continuing the cycle of cold water entrainment. The model recreates the winter conditions in 2003/2004 reasonably well, perhaps because the T-min was already fully eroded in the September 2003 initialization profile.

The model results suggest that both surface forcing and lateral processes are important for maintaining the vertical temperature structure in the Aleutian Basin. Without adequate cooling and mixing from above, the T-min layer will not be fully formed and will be unable to persist between the warmer layers above and below it. In the absence of a lateral heat source, the T-max layer will slowly erode. A combination of weak atmospheric forcing at the surface and increased lateral advection may destroy the temperature inversion characteristic of the Aleutian Basin, as occurred in winter 2002/2003. Furthermore, the existing vertical structure at the onset of winter mixing appears to play an important role in the temperature and depth of the new winter's mixed layer via the reemergence mechanism (Deser et al. 2003), as evidenced in the float data for 2003/2004 and perhaps in the NCEP/NCAR reanalysis SST product for 1979/1980, 1983/1984, as well as 2003/2004.

8. Summary and Discussion

Oceanographic data from profiling CTD floats indicate that the thermohaline structure of the southeast Aleutian Basin underwent major changes between August 2001 and August 2004. The data analyzed and presented here show a warming and freshening of the mixed-layer waters, warming of the subsurface, and the virtual disappearance of the subsurface temperature inversion characteristic of the region. A variety of factors contributed to the loss of this structure, including weak winds in winter 2003, unusually shallow mixing, weak heat loss, and a circulation anomaly which delivered warm, relatively fresh water to the surface and warm, relatively salty water to the subsurface ocean in the region during winter 2002/2003.

The change in Turner Angle through the upper water column is related to the disappearance of the T-min. In the early portion of the data set, the interface between the T-min and T-max was diffusively unstable in the mean, with Turner Angles occasionally indicating strong diffusive instability characteristic of cold fresh water overlying warm salty water. There is little evidence of any diffusive instability in the later portion of the time series, reflecting diminishment, sometimes to the point of absence, of the temperature inversion after early 2003. While diffusive instability doubtless increases vertical mixing between the T-max and the T-min, the significance of diffusive instability's role in this diminishment remains an open question.

The increased temperature and decreased winter mixed-layer depth in the southeast Aleutian Basin during winter 2002/2003 are likely the combined result of local atmospheric forcing and increased inflow of relatively warm Alaskan Stream water into the region. The warming trend began early in the data set, consistent with the weak winds and weak ocean heat flux losses for the entire 2002/2003 cooling season. These conditions combined to inhibit deep winter mixing. The result was an anomalously warm, fresh, light, shallow winter mixed layer which did not create the usual spring T-min layer. The most telling evidence in the float data for

a circulation anomaly in the Alaskan Stream and ANSC is the expansion and warming of the T-max layer in the southeast Aleutian Basin. Without increased warm water transport at the subsurface level, the T-max probably would not have increased in temperature as observed, even without a strong T-min to counteract it. The combined effect of weak initial formation and increased erosion from below by an invigorated T-max led to the full loss of the T-min layer by late spring 2003.

Interannual freshening of the mixed layer could be a result of the decreased winter mixing depth and density in winter 2002/2003. Many factors could have contributed to the mixed-layer freshening, including increased inflow of fresh water from the Alaskan Stream into the region, anomalous air-sea fresh water flux, decreased entrainment from the halocline below, changes in ice melt or stream flow, and variations in cross-shelf exchange. NCEP/NCAR reanalysis freshwater flux product values (not shown) have cooling season anomalies in the wrong sense for the observed mixed-layer changes, and they are very uncertain. The other possible contributors are very difficult to quantify. However, because the mixed-layer salinity anomaly with respect to the seasonal cycle (Figure 5) only freshened during the winter of 2002/2003, it seems at least feasible that weak winter mixed layer entrainment then contributed to the salinity trend. The low wind stress and weak heat loss during the 2002/2003 cooling season in the southeast Aleutian Basin certainly combined to form a shallow mixed layer, inhibiting entrainment of cold salty water from the halocline. The reduced wintertime entrainment of halocline water may have kept the mixed layer fresher and thus lighter than normal for this time of year, creating a feedback mechanism to increase stability and decrease the depth of convective mixing, supplying less salty water to the mixed-layer. The fresh mixed-layer values continue through the rest of the time series, suggesting that a single anomalous winter

may have effects in the following seasons. This phenomena has also been observed on the eastern shelf of the Bering Sea (Stabeno et al., 2001)

The Sea Level Pressure (SLP) pattern in winter 2002/2003 does not correspond to the normal wind patterns expected in either the positive or negative phase of the PDO (Bond et al., 2003). Instead, the SLP pattern displays a single low-pressure center over the North Pacific with anomalously warm SSTs along the coast and in the Bering Sea. The single low pressure in winter 2002/2003 was located south of Alaska, and only slightly east of its normal position, so that cyclonic circulation delivered warmer maritime air from the North Pacific via southerly winds, rather than cold air from the north (Nick Bond, personal communication). The correlations among winds, SST, and heat flux anomalies are further evidence for a northward shift in the Alaskan Stream and resultant positive transport anomaly into the basin. It is also possible that the water-properties feeding into the Bering Sea changed, but it has been argued (Reed, 1995) that changes of transport through the passes is a more likely source of variability.

The anomalous atmospheric conditions and circulation pattern studied here may also be attributable in part to the relatively weak El Niño of 2002/2003. One mechanism of ENSO related variability in the North Pacific is the position and strength of the Aleutian Low. During El Niño years, the Aleutian Low generally deepens and moves south and east (Alexander et al., 2002). Niebauer (1988) speculated that weak El Niños may have a larger impact on the North Pacific and the Bering Sea than do strong events. The displacement of the Aleutian Low in response to the strong 1982/1983 El Nino was far to the south and east, compared to normal conditions and previous El Nino years (Niebauer, 1988). The far-eastward position of the low-pressure system resulted in the circulation of a cold air mass over the Bering Sea. Although the associated winds originated in the North Pacific as they do during warm events, the position of

the low caused the winds to blow into the Bering Sea from the Alaskan land mass, bringing cold air into an already cold system. Conversely, in 1997/1998 and in 2002/2003 the displacement of the Aleutian low was not as far to the southeast, so that the cyclonic circulation transported moderate maritime air directly to the Bering Sea. The single low pressure system which dominated the North Pacific in winter 2002/2003 (Bond et al., 2003) most likely served to create upper air circulation which contributed to high temperatures along the west coast of North America and in the Bering Sea.

Coastally trapped waves that travel north along the west coast of North America, into the North Pacific are another possible teleconnection mechanism from the tropics (Alexander et al., 2002). A coastally trapped wave may be the cause of the SSHA pattern seen in November 2002 - January 2003 (Figure 12), strengthening the Alaskan Stream and allowing anomalous warm water flow into the Bering Sea. Equatorial Kelvin wave activity is certainly enhanced during El Niños. The SSHA pattern observed in winter 2002/2003 also occurred during the 1997/1998 winter, the first strong El Niño winter for which satellite altimeter data are available. Furthermore, similar anomalies are not as prevalent in the SSHA maps for La Niña and neutral years. However, the wave could also be locally forced in the Gulf of Alaska or along the American west coast, and reinforced by the along-peninsula wind anomalies discussed earlier.

Significant and linked oceanic and atmospheric anomalies in the southeast Aleutian Basin of the Bering Sea during winter 2002/2003 have been analyzed in this study. The impacts of such anomalies on the ecological systems in the region are less clear. The loss of the T-min layer in winter 2002/2003 may have significant impacts on biota (Reed, 1995). In a study of data collected at Ocean Station Papa (50^{o}N, 145^{o}W), Freeland et al. (1997) found that SST temperatures increased and salinity decreased over the course of 60 years between 1935 and

1995. The study speculated that the increased surface stratification and resultant decrease in winter mixed-layer depth led to a reduction of nutrient replenishment to the upper ocean, thereby causing a possible decrease in productivity. While the time-series analyzed here is much shorter, regional ecological changes could have strong economic impacts, as the Bering Sea Shelf adjacent to the Aleutian Basin is among the most productive fisheries regions in the world. Greater understanding of the physical dynamics of the Aleutian Basin and the ecological impacts of changes in the dynamics will come with increased data collection. Data continue to be collected by the profiling CTD floats throughout the deep basin. Analysis of winter 2003/2004 indicates a persistence of the warming, and an even weaker T-min formation than 2002/2003 despite more normal surface forcing in the latter year. The evolving conditions in the subsurface structure will be of interest from both scientific and socio-economic perspectives in the near and distant future.

Acknowledgments: AEW performed much of this research as part of her Master in Science at the University of Washington and was supported by an advanced education grant from the U.S. Coast Guard. The NOAA National Marine Fisheries Steller Sea Lion Coordinated Research Program and the NOAA Office of Oceanic and Atmospheric Research support the float array and GCJ, respectively. The floats were fabricated, ballasted, and tested by Prof. Stephen Riser's group at the University of Washington. NCEP/NCAR reanalysis products provided by the NOAA-CIRES Climate Diagnostics Center, Boulder Colorado, USA from their Web site at http://www.cdc.noaa.gov. The altimeter products were produced by CLS Space Oceanography Division as part of the Environment and Climate EU ENACT project (EVK2-CT2001-00117) and with support from CNES from their web site at http://www.aviso.oceanobs.com. This work

benefited from conversations with Drs. Phyllis Stabeno and Carol Ladd. The manuscript was improved by thoughtful comments from two anonymous referees. This is Pacific Marine Environmental Laboratory contribution number 2715.

REFERENCES

Alexander, M. A., I. Blade, F. R. Lanzante, N. Lau, and J. D. Scott. 2002. The atmospheric bridge: The influence of ENSO teleconnections on air-sea interaction over the global ocean. Journal of Climate, *15*, 2205-2231.

Bond, N. A., and J. M. Adams. 2002. Atmospheric forcing of the southeast Bering Sea Shelf during 1995-1999 in the context of a 40-year historical record. Deep-Sea Research II, *49*, 5869-5887.

Bond, N. A., J. E. Overland, M. Spillane, P. J. Stabeno. 2003. Recent shifts in the state of the North Pacific. Geophysical Research Letters, *30*, 2183-2186.

Cleveland, W. S., and S. J. Devlin. 1988. Locally weighted regression: An approach to regression analysis by local fitting. Journal of the American Statistical Association, *83*, 596-610.

Cokelet, E. D., and P .J. Stabeno. 1997. Mooring observation of the thermal structure, salinity, and currents in the SE Bering Sea basin. Journal of Geophysical Research, *102*, 22,947-22,964.

Deser, C., M. A. Alexander, and M. S. Timlin. 2003. Understanding the persistence of sea surface temperature anomalies in midlatitudes. Journal of Climate, *16*, 57-72.

Ducet, N., P.-Y. Le Traon, and G. Reverdin. 2000. Global high resolution mapping of ocean circulation from Topex/Poseidon and ERS-1 and -2. Journal of Geophysical Research, *105*, 19477-19498.

Endoh, T., H. Mitsudera, S.-P. Xie, and B. Qiu. 2004. Thermohaline structure in the subarctic North Pacific simulated in a general circulation model. Journal of Physical Oceanography, *34*, 360-371.

Freeland, H., K. Denman, C. S. Wong, F. Whitney, and R. Jaques. 1997. Evidence of change in the winter mixed layer in the Northeast Pacific Ocean. Deep-Sea Research I, *44*, 2117-2129.

Johnson, G. C., P. J. Stabeno, and S. D. Riser. 2004. The Bering Slope Current system revisited. Journal of Physical Oceanography, *34*, 384-398.

Kalnay, E., M. Kanimitsu, R. Kistler, W. Collins, D. Deaven, L. Gandin, M. Iredell, S. Saha, G. White, J. Woolen, Y. Zhu, A. Leetmaa, and B. Reynolds. 1996. The NCEP/NCAR 40-year reanalysis project. Bulletin of American Meteorological Society, *77(3)*, 437-472.

Kinder, T. H., L. K. Coachman, and J. A. Galt. 1975. The Bering Slope Current system. Journal of Oceanography, *5*, 231-244.

Kistler, R., E. Kalnay, W. Collins, S. Saha, G. White, J. Woolen, M. Chelliah, W. Ebisuzaki, M. Kanamitsu, V. Kousky, H. van den Dool, R. Jeene, M. Fiorino. 2001. The NCEP-NCAR 50-Year reanalysis: Monthly Means CD-ROM and Documentation. Bulletin of the American Meteorological Society, *82*, 2, 247-267.

Ladd, C., and N. A. Bond. 2002. Evaluation of the NCEP/NCAR reanalysis in the NE Pacific and Bering Sea. Journal of Geophysical Research, *107*, 3158, doi: 10.1029/2001JC001157.

Lozier, M. S., W. B. Owens, and R. G. Curry. 1995. The climatology of the North Atlantic. Progress in Oceanography, 36, 1-44.

Mantua, N. J., S. R. Hare, Y. Zhang, J. M. Wallace and R. C. Francis. 1997. A Pacific interdecadal climate oscillation with impacts on salmon production. Bulletin of the American Meteorological Society, *78*, 6, 1069-1079.

Miura, T., S. Suga and K. Hanawa. 2002. Winter mixed layer and formation of dichothermal water in the Bering Sea. Journal of Oceanography, *58*, 815-823.

Miura, T., S. Suga and K. Hanawa. 2003. Numerical study of formation of dichothermal water in the Bering Sea. Journal of Oceanography, *59*, 369-376.

Moisan, J. R. and P. P. Niiler. 1998. The seasonal heat budget of the North Pacific: Net heat flux and heat storage rates (1950-1990). Journal of Physical Oceanography, *28*, 401-421.

Niebauer, H. J. 1988. Effects of El-Nino Southern Oscillation and North Pacific weather patterns on interannual variability in the subarctic Bering Sea. Journal of Geophysical Research, 93, 5051-5068.

Price, J. F., R. A. Weller, and R. Pinkel. 1986. Diurnal cycling: Observations and models of the upper ocean response to diurnal heating, cooling, and wind mixing. Journal of Geophysical Research, *91*, 8411-8427.

Reed, R. K., 1990. A year long observation of water exchange between the North Pacific and the Bering Sea. Limnology and Oceanography, *35(7)*, 1604-1609.

Reed, R. K, and P. J. Stabeno. 1994. Flow along and across the Aleutian Ridge. Journal of Marine Research, 52, 639-648.

Reed, R. K. 1995. On the variable subsurface environment of fish stocks in the Bering Sea. Fisheries Oceanography, *4:4*, 317-323.

Reed, R.K. and P.J. Stabeno. 1999. The Aleutian North Slope Current. T.R. Loughlin and K. Ohtani Eds., Dynamics of the Bering Sea: A Summary of Physical, Chemical and Biological

Characteristics, and a Synopsis of Research on the Bering Sea, Sydney, British Columbia and Fairbanks, Alaska: North Pacific Marine Science Organization (PISCES) and University of Alaska Sea Grant, AK-SG-99-03, 177-191.

Roden, G. I. 1995. Aleutian Basin of the Bering Sea: Thermohaline, oxygen, nutrient, and current structure in July 1993. Journal of Geophysical Research, *100*, 13,593-13,554.

Ruddick, B. 1983. A practical indicator of the stability of the water column to double-diffusive activity. Deep Sea Research, *30*, 1105-1107.

Sayles, M. A., K. Aagaard, and L. K. Coachman. 1980. Oceanographic atlas of the Bering Sea Basin. University of Washington Press, Seattle, 158 pp.

Schudlich, R. S, and J. F. Price, 1992. Diurnal cycles of current, temperature, and turbulent dissipation in a model of the equatorial upper ocean. Journal of Geophysical Research, 97, 5409-5422.

Stabeno, P. J., N. A. Bond, N. B. Kachel, S. A. Salo, and J. D. Schumacher. 2001. On the temporal variability of the physical environment over the south-eastern Bering Sea. Fisheries Oceanography, *10:1*, 81–98.

Stabeno, P. J., G. L. Hunt, Jr., J. M. Napp, and J. D. Schumacher. In press. Interdisciplinary ocean science of the Bering Sea Continental Shelf. In The Sea, Vol. 14—The Global Coastal Ocean: Interdisciplinary Regional Studies and Syntheses, John Wiley & Sons, Inc.

Stabeno, P. J., and R. K. Reed. 1992. A major circulation anomaly in the western Bering Sea. Geophysical Research Letters, *19*, 763-773.

Stabeno, P. J., and R. K. Reed. 1994. Circulation in the Bering Sea Basin observed by satellite-tracked drifters: 1986-1993. Journal of Physical Oceanography, *24*, 848-854.

Stabeno, P. J., J. D. Schumacher, and K. Ohtani. 1999. The physical oceanography of the Bering Sea. T.R. Loughlin and K. Ohtani Eds., Dynamics of the Bering Sea: A Summary of Physical, Chemical and Biological Characteristics, and a Synopsis of Research on the Bering Sea, Sydney, British Columbia and Fairbanks, Alaska: North Pacific Marine Science Organization (PISCES) and University of Alaska Sea Grant, AK-SG-99-03, 1-28.

Takenouti, A. Y., and K. Ohtani. 1974. Currents and water masses in the Bering Sea: A review of Japanese work. In Oceanography of the Bering Sea: with emphasis on renewable resources. University of Alaska, Fairbanks, Institute of Marine Science, Occasional Publication, *2*, 39-57.

Wong, A. P. S., G. C. Johnson, G. C., and W. B. Owens. 2003. Delayed-mode calibration of autonomous CTD profiling float salinity data by θ–S climatology. Journal of Atmospheric and Oceanic Technology, *20*, 308-318.

FIGURE CAPTIONS

Figure 1. Bering Sea geography. Major connections between the deep basins of the Bering Sea and the North Pacific include (west to east, indicated by triangles) Kamchatka Strait, Near Strait, Amchitka Pass, and Amukta Pass. Float CTD profile locations (grey plusses) are indicated along with the mapping location (pentagram). Areas shallower than 1000 m are lightly shaded, with land more darkly shaded. The thick line separates data in the southeast Aleutian Basin from the rest of the deep Bering Sea.

Figure 2. Mixed-layer potential temperature (top left), salinity (top right), potential density anomaly (bottom left), and pressure at the base of the mixed layer (bottom right) plotted versus time using the float CTD data (plusses) in the southeast Aleutian Basin (Figure 1) with seasonal cycles (solid lines) estimated from annual and semiannual harmonics fit to these data.

Figure 3. Time-pressure sections of potential temperature (top) contoured in color at 0.5^{o}C intervals and 0.1^{o}C intervals between 3.5 and 4^{o}C (dotted lines) and salinity (bottom) contoured in color at 0.1 intervals from a loess fit of the float CTD data to 55^{o}N, 174^{o}W. Red values are high and blue values low. Potential density anomaly contours at 0.2 kg m^{-3} intervals are overlaid in white.

Figure 4. Turner Angles estimated from float CTD data in the southeast Aleutian Basin (Figure 1). Mean values (thick line) with one standard deviation envelope (thin lines) plotted against potential density anomaly (left). Raw values (plusses) on σ_θ = 26.65 kg m^{-3} plotted versus time

(right). Turner Angles below –45^{o} are increasingly diffusively unstable, with strong instability found below –71.6^{o}.

Figure 5. Mixed-layer potential temperature (left) and salinity (right) anomalies in the southeast Aleutian Basin calculated from the difference of the data and seasonal cycles in Figure 2. Raw values (plusses) are fit with a one-dimensional loess filter with a one-year half-power point (solid lines).

Figure 6. Potential temperature values of the T-min (plusses) from float CTD data in the southeast Aleutian Basin, as well as the T-max (circles) plotted versus time (left). Mean potential temperature-salinity (θ–S) relationships for 2002 (thin black line) and 2003 (thick grey line) in the region with potential density anomaly contours (dotted lines) overlaid at 0.2 kg m^{-3} intervals (right).

Figure 7. Values of potential temperature (left) and pressure (right) on σ_{θ} = 26.6 kg m^{-3} from float CTD data in the southeast Aleutian Basin (Figure 1).

Figure 8. Mean NCEP/NCAR reanalysis net heat flux (top) and wind stress (bottom) products from 1958/1959 to 2003/2004 at 55^{o}N, 174^{o}W averaged over each cooling season (21 September - 10 April). Values for 1958/1959 are plotted at 1959 (pentagrams joined by solid line) and so on. The overall mean (horizontal solid line) is between those lines prior to and after 1979 (horizontal dot-dashed lines) when satellite data assimilation began. The 1977 regime shift of the Pacific Decadal Oscillation (vertical dashed line) is indicated.

Figure 9. Mean NCEP/NCAR reanalysis sea surface temperatures (SST) product values from 1958/1959 to 2003/2004 at 55°N, 174°W averaged over each cooling season. Details follow Figure 8.

Figure 10. Heat content integrated to $\sigma_\theta = 26.7$ kg m^{-3} from the float CTD data (grey plusses) in the southeast Aleutian Basin (Figure 1) mapped to 55°N, 174°W (thick line) and compared with NCEP/NCAR reanalysis surface heat flux product interpolated to that location and time-integrated over that period (thin line).

Figure 11. Mean NCEP/NCAR reanalysis along-peninsula wind stress (positive towards 75°T) product at 53°N, 173°W from 1958/1959 to 2003/2004 averaged over each cooling season.

Figure 12. Monthly averages of satellite altimeter sea surface height anomaly (SSHA) maps from CLS starting in October 2002 (bottom) and ending in January 2003 (top), color contoured at 5 cm intervals (scale at top). Land (gray shading) and the 1000-m isobath (thick white line) are overlaid.

Figure 13. Pressure-time sections of potential temperature (top) and salinity (bottom) simulated with a one-dimensional model (Price et al., 1986). Presentation details follow Figure 3. The model is reinitialized with float CTD data mapped to 55°N, 174°W at 1 September of each year, and then run for 12 months forced by NCEP/NCAR reanalysis surface flux products interpolated to that location.

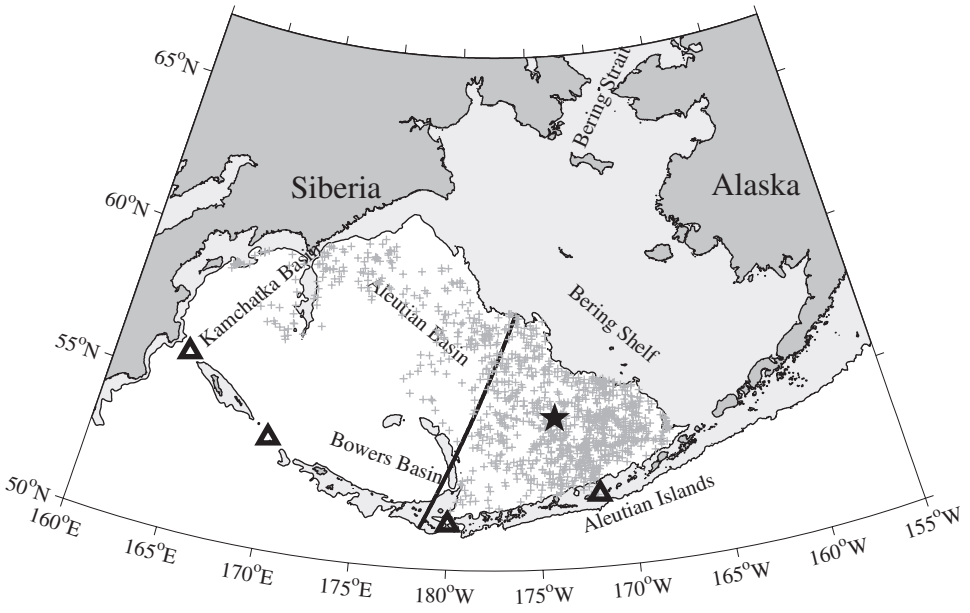
65°N
60°N
55°N
50°N
160°E
165°E
170°E
175°E
180°W
175°W
170°W
165°W
160°W
155°W
Siberia
Alaska
Bering Strait
Kamchatka Basin
Aleutian Basin
Bering Shelf
Bowers Basin
Aleutian Islands

Figure 1

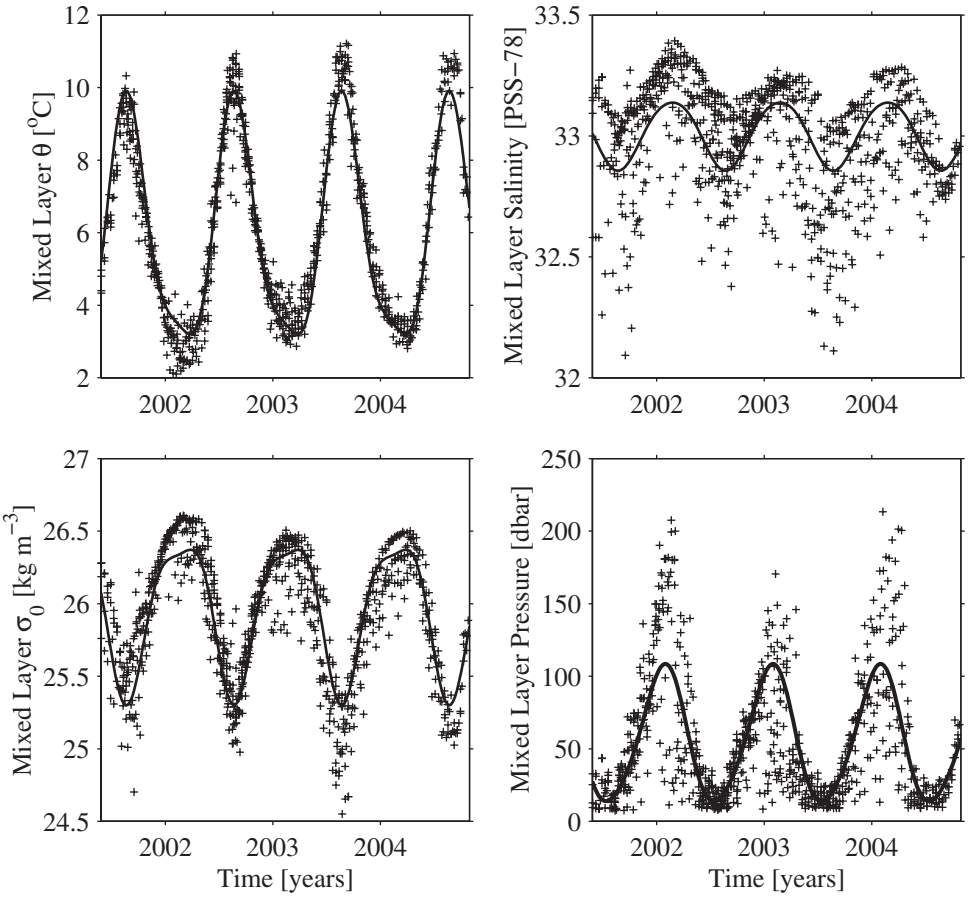
Mixed Layer θ [°C]
Mixed Layer Salinity [PSS−78]
Mixed Layer σ0 [kg m−3]
Mixed Layer Pressure [dbar]
Time [years]
Time [years]
2002
2003
2004

Figure 2

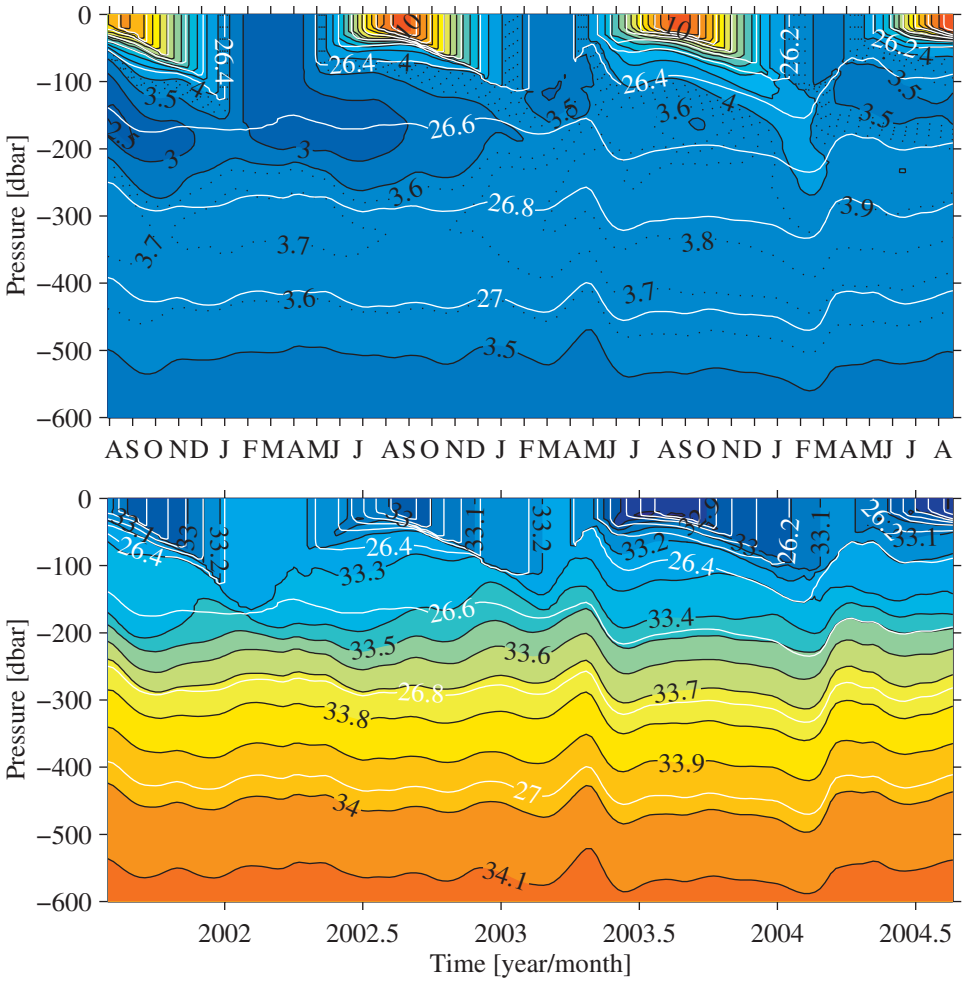
Pressure [dbar]
0
−100
−200
−300
−400
−500
−600
A S O N D J F M A M J J A S O N D J F M A M J J A S O N D J F M A M J J A
26.4
26.6
26.8
27
3.5
3.6
3.7
3.8
3.9
33.1
33.2
33.3
33.4
33.5
33.6
33.7
33.8
33.9
34
34.1
2002
2002.5
2003
2003.5
2004
2004.5
Time [year/month]

Figure 3

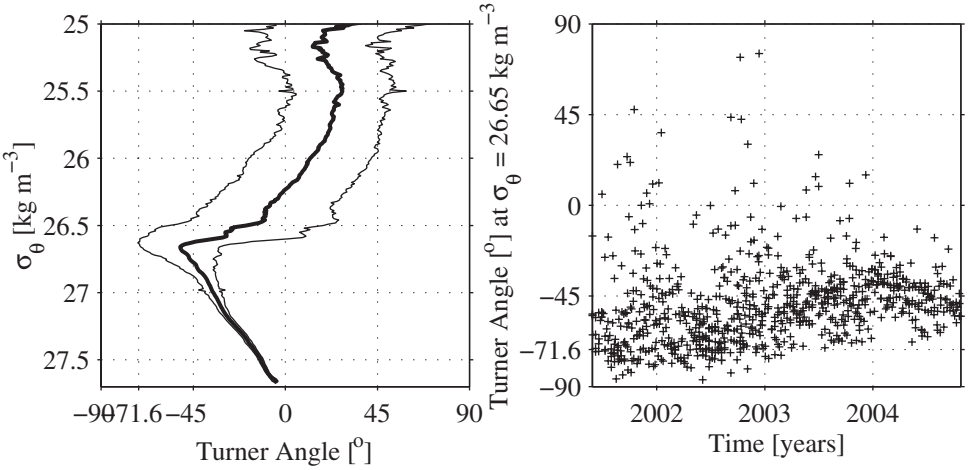
25
25.5
26
26.5
27
27.5
σθ [kg m−3]
−90
−71.6
−45
0
45
90
Turner Angle [o]
Turner Angle [o] at σθ = 26.65 kg m−3
90
45
0
−45
−71.6
−90
2002
2003
2004
Time [years]

Figure 4

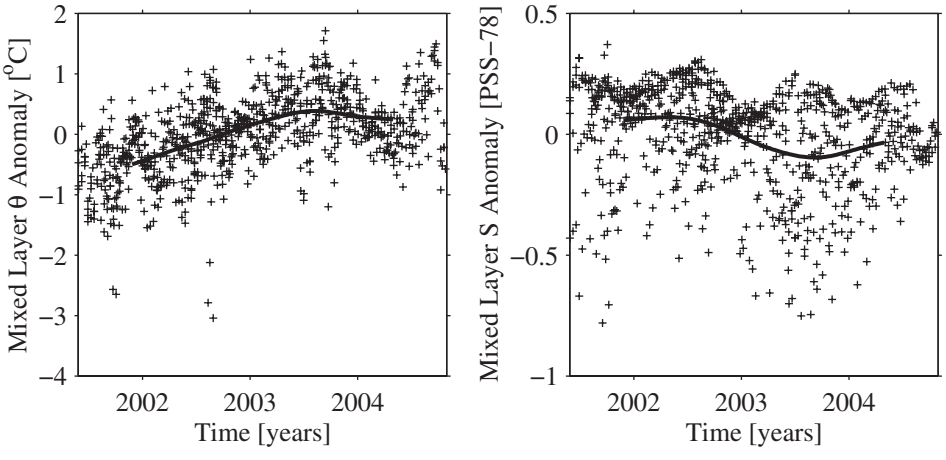
Mixed Layer θ Anomaly [°C]
2
1
0
−1
−2
−3
−4
2002
2003
2004
Time [years]
Mixed Layer S Anomaly [PSS−78]
0.5
0
−0.5
−1
2002
2003
2004
Time [years]

Figure 5

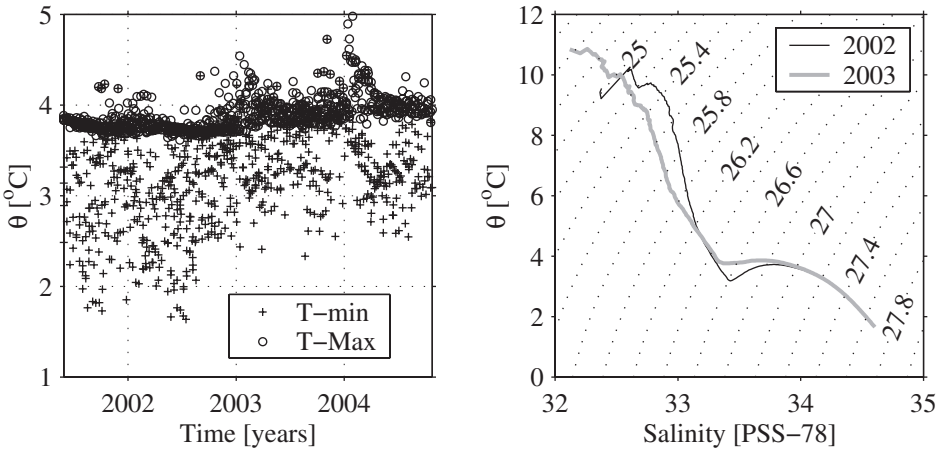
5
4
3
2
1
θ [°C]
T−min
T−Max
2002
2003
2004
Time [years]
12
10
8
6
4
2
0
θ [°C]
2002
2003
25
25.4
25.8
26.2
26.6
27
27.4
27.8
32
33
34
35
Salinity [PSS−78]

Figure 6

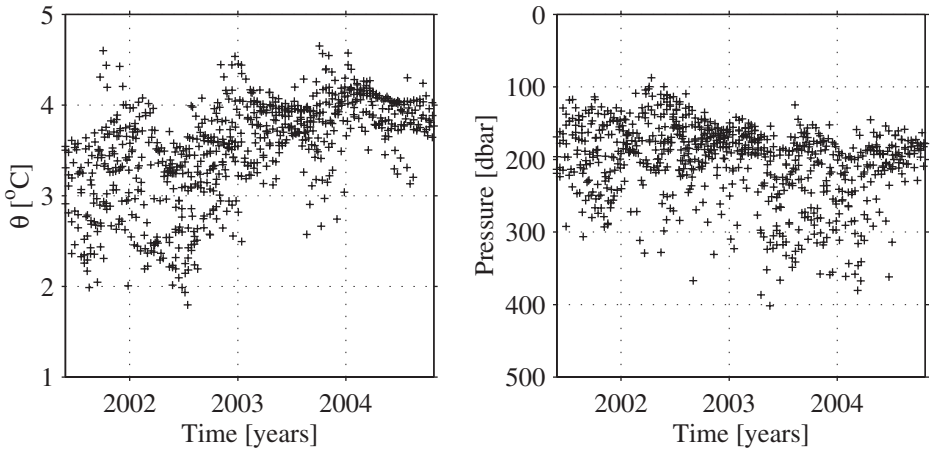
5
4
3
2
1
θ [°C]
2002
2003
2004
Time [years]
0
100
200
300
400
500
Pressure [dbar]
2002
2003
2004
Time [years]

Figure 7

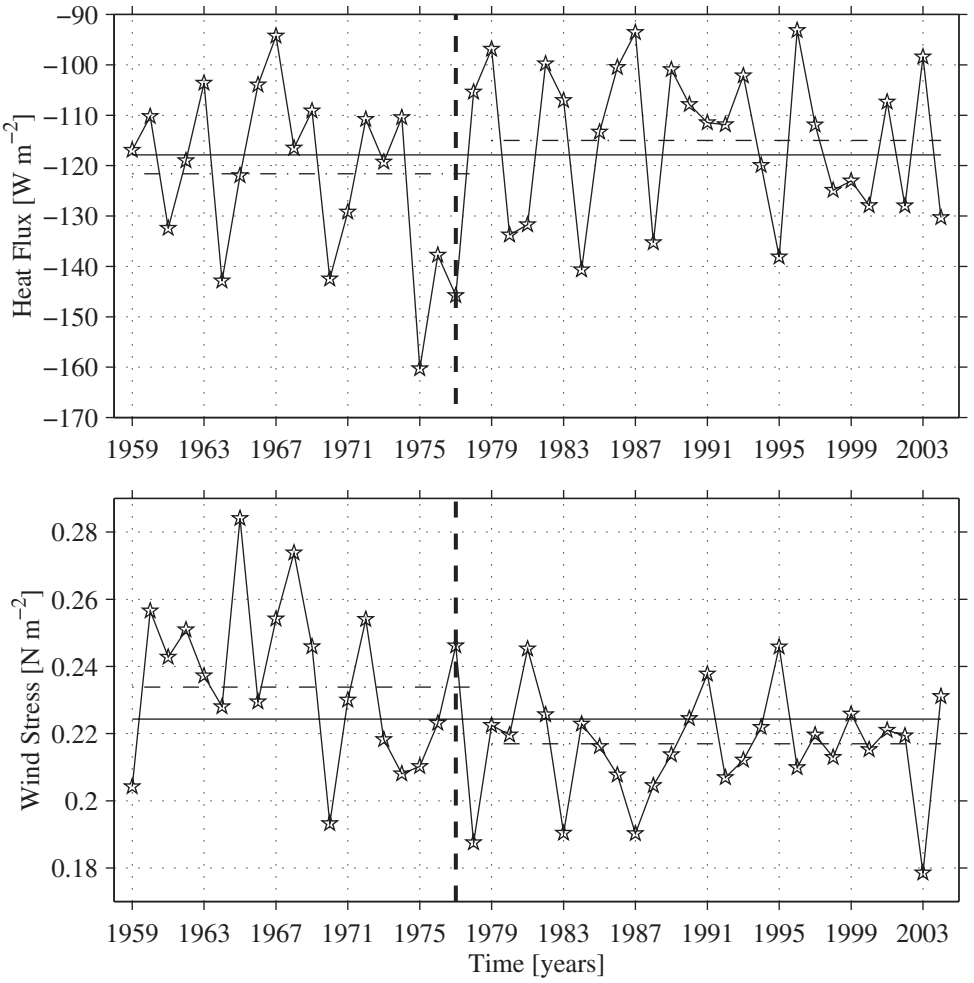
−90
−100
−110
−120
−130
−140
−150
−160
−170
Heat Flux [W m^{-2}]
1959
1963
1967
1971
1975
1979
1983
1987
1991
1995
1999
2003
0.28
0.26
0.24
0.22
0.2
0.18
Wind Stress [N m^{-2}]
Time [years]

Figure 8

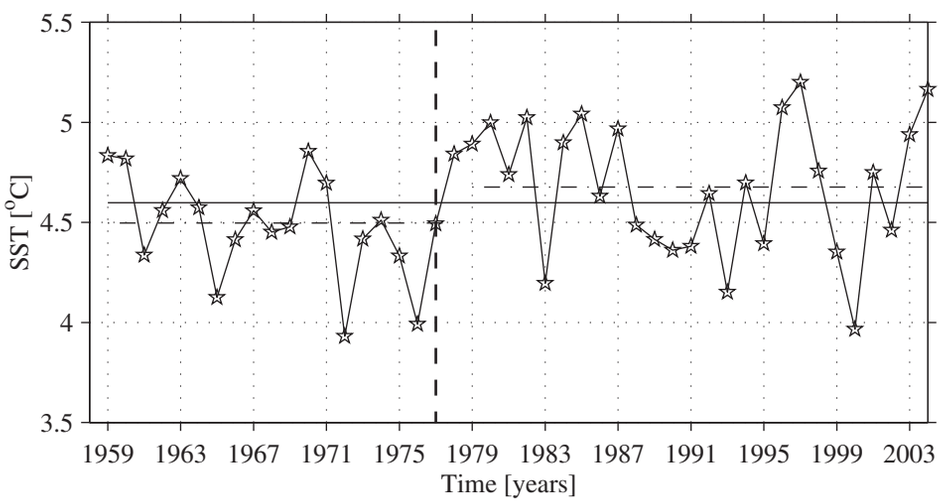
5.5
5
4.5
4
3.5
SST [°C]
1959
1963
1967
1971
1975
1979
1983
1987
1991
1995
1999
2003
Time [years]

Figure 9

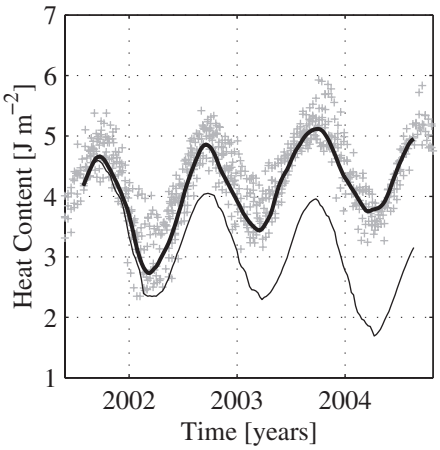

Figure 10

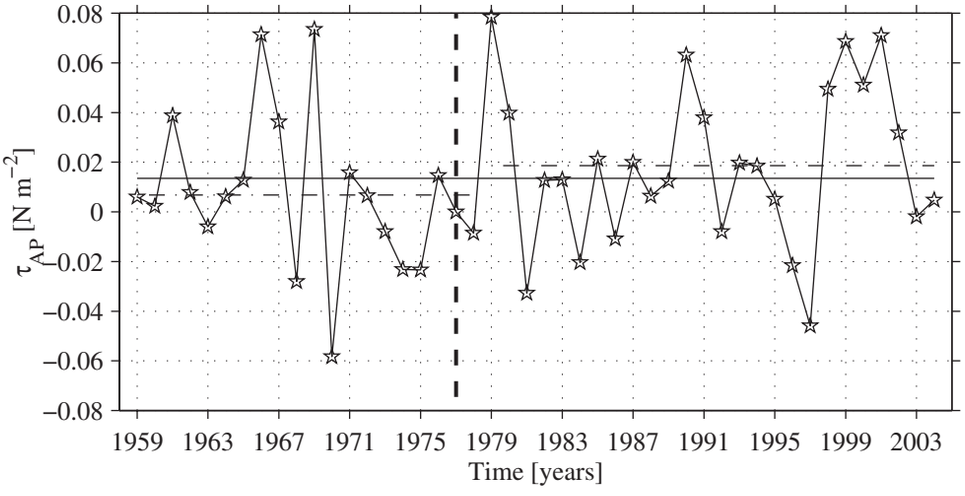
0.08
0.06
0.04
0.02
0
−0.02
−0.04
−0.06
−0.08
τ_{AP} [N m^{-2}]
1959
1963
1967
1971
1975
1979
1983
1987
1991
1995
1999
2003
Time [years]

Figure 11

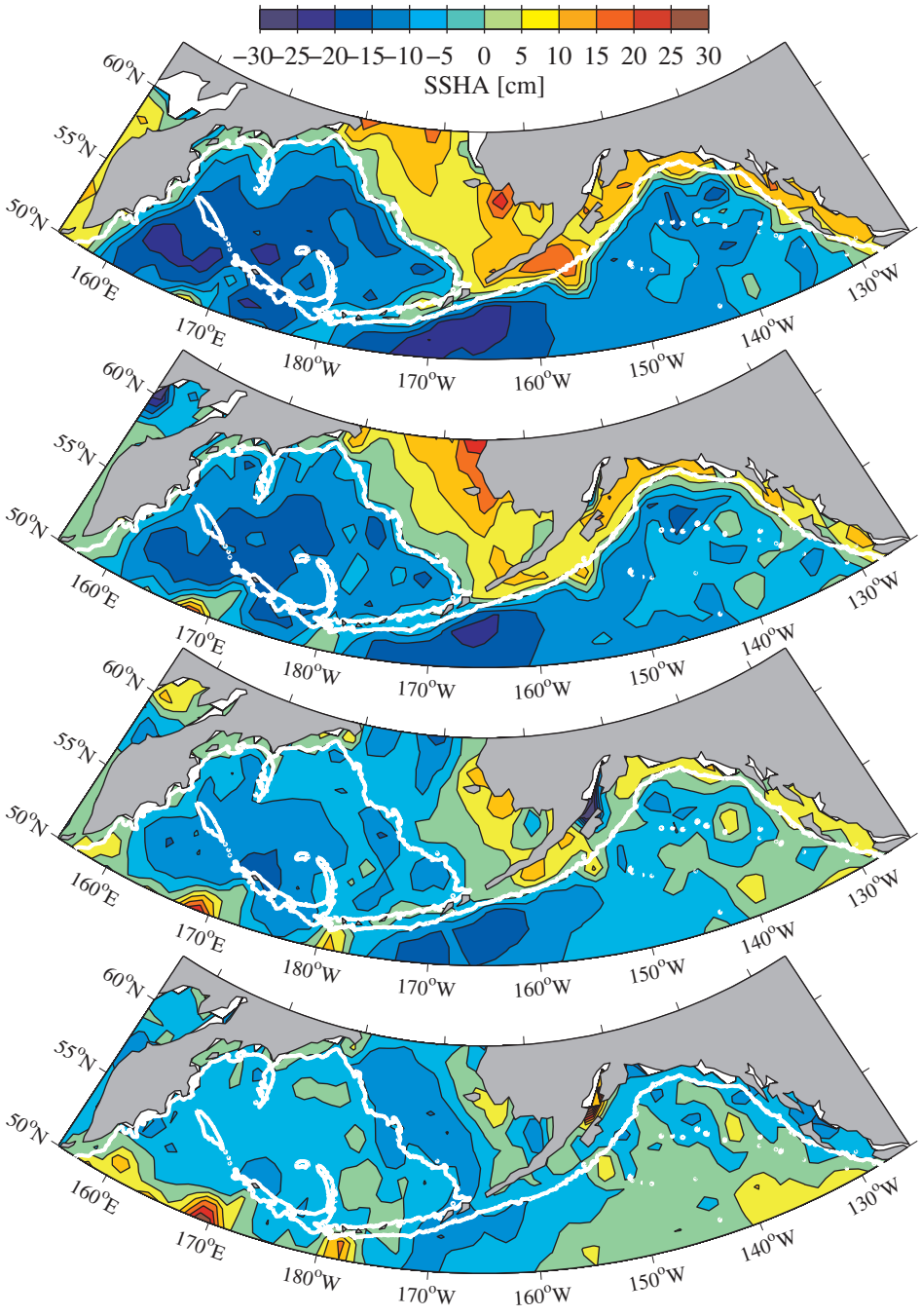
−30 −25 −20 −15 −10 −5 0 5 10 15 20 25 30
SSHA [cm]
60°N
55°N
50°N
160°E
170°E
180°W
170°W
160°W
150°W
140°W
130°W

Figure 12

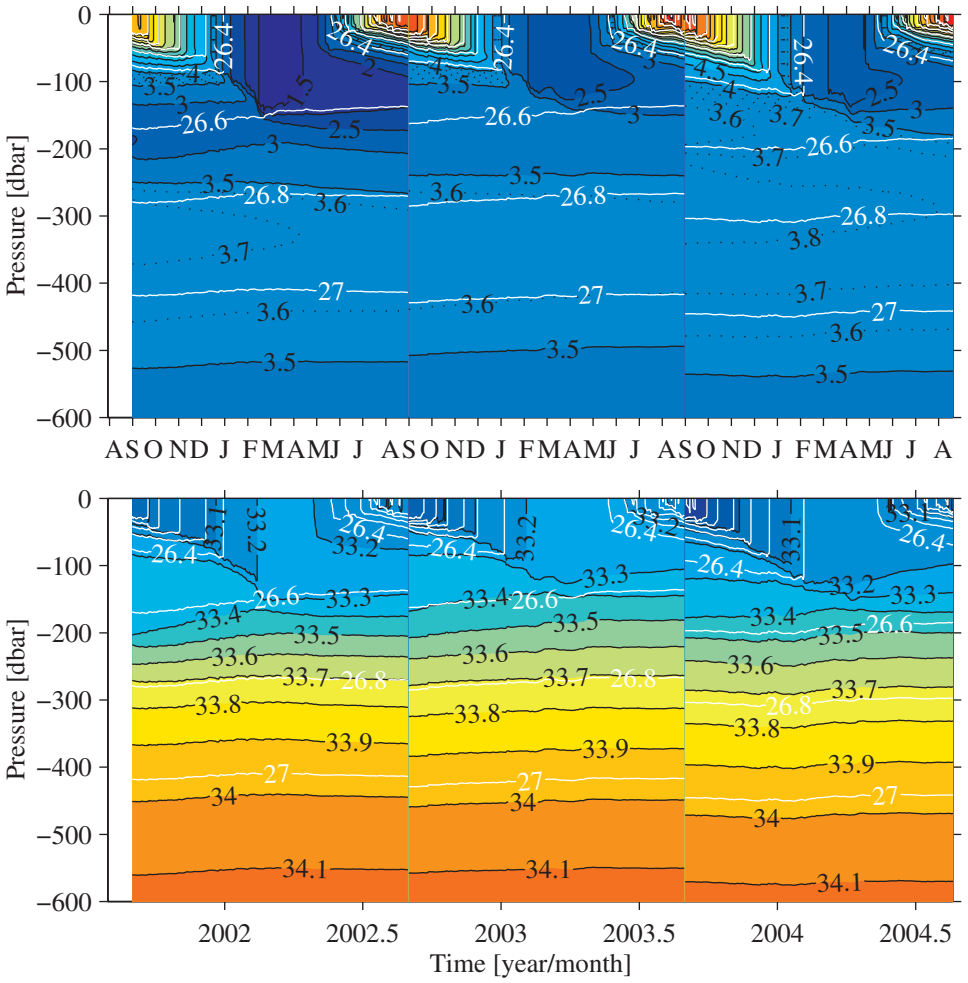
Pressure [dbar]
0
−100
−200
−300
−400
−500
−600
ASO ND J FMAMJ J ASO ND J FMAMJ J ASO ND J FMAMJ J A
2002
2002.5
2003
2003.5
2004
2004.5
Time [year/month]

Figure 13